ARMA 18–503

Pre- and Post-Fracturing Analysis of a Hydraulically Stimulated Reservoir

Erfan Sarvaramini
Department of Civil and environmental Engineering, University of Waterloo, Waterloo, ON, Canada
Robert Gracie
Department of Civil and environmental Engineering, University of Waterloo, Waterloo, ON, Canada
Maurice Dusseault
Earth and Environmental Sciences Department, University of Waterloo, Waterloo, ON, Canada

ABSTRACT: It is widely recognized that the hydraulic fracturing operation in naturally fractured rocks leads to creation of a stimulated zone of increased conductivity through shear reactivation of natural fractures, irreversible plastic deformation, and induced bulk damage. The characterization of the Stimulated Volume (SV) can improve the fracture design and subsequent well performance. However, there still remain considerable uncertainty with respect to the shape, size, and conductivity of the stimulated volume, as these characteristics are strongly dependent upon the distribution of natural fractures, in-situ stresses, and other reservoir and fluid parameters. In this work, we introduce a non-local poro-elasto-plastic zone model of enhanced permeability for the SV, with a characteristic length scale controlled by the orientation and density of the fracture network. We first quantify the evolution of the SV and pressure change in the reservoir for a typical example of hydraulic fracture stimulation in a tight formation. After the creation of a sufficient stimulated volume, the well is shut-in for an extended period of time and the wellbore pressure is allowed to fall-off. Using the existing analytical solution for the finite conductive fracture, the flow capacity of the stimulated zone is calculated.

1. INTRODUCTION

Development of the shale reservoirs involves the use of horizontal wells stimulated via hydraulic fracturing (HF) (Economides and Nolte, 2000). During HF a working fluid is injected into a target formation at high rates and pressures causing deformation and failure (fracture) of the rock mass and increasing the permeability in a region surrounding the injection point creating a Stimulated Volume (SV) (Cipolla et al. 2010 and Mayerhofer et al., 2010).

Microseismic imaging is a primary tool to estimate the extent of the complex hydraulic fracturing and SV evolution in hydraulically stimulated tight formations (Maxwell, 2014, Dusseault et al. 2011) (Fig. 1a). Microseismic events are usually collected on the near-surface geophones to measure the seismic energy release associated with shear breakage of the rocks along the pre-existing natural fractures. (i.e., Mode II and Mode III fracturing). The shear fracturing effects (seismic and aseismic deformations) result in a stimulated region of naturally self-propped fractures (i.e., a shear dilation zone) spanning a large volume of the target reservoir formation (Fig. 1a) (Dusseault, 2013). The size of the micorsiemic clouds is often considered as the effective SV and shear dilation zone. However, microseismic rarely provides any information on the dynamic of fracturing, fluid flow and stimulated permeability. In addition, the total energy of microseismic waves is often negligible compared to the total hydraulic fracturing input energy suggesting that most of the shear slip events are aseismic (Boroumand and Eaton, 2012) Hence, the development of a comprehensive geomechanical model which can explain the complex fracturing of Mode II and Mode III deformation can constrain the size of the SV and provide a more consistent micorsiemic interpretation.

In addition to the Mode II and Mode III fracturing, the hydraulic fracturing stimulation must also create tensile fractures (Mode I) to accommodate large injection fluid and proppant volumes. The propagation of tensile fractures can significantly increase the shear stress in the macroscopic vicinity of the fracture tips, at a scale of meters or tens of meters, depending on the fracture aperture and curvature. This may lead to shear slip events along the pre-existing fractures intersecting or close to the propagating tensile crack, effectively altering fracture direction, bifurcating the crack front, or at the least leading to some irreversible volume change through shear dilation (affecting the local stresses). As the result, the

fracture network can be quite complex on the length scale of the strong local fabric. This zone which is mostly dominated by the Mode I tensile fracture deformation, is called the “sand" zone because it is the zone that can be propped with injected sand (Fig. 1b) (Dusseault, 2013).

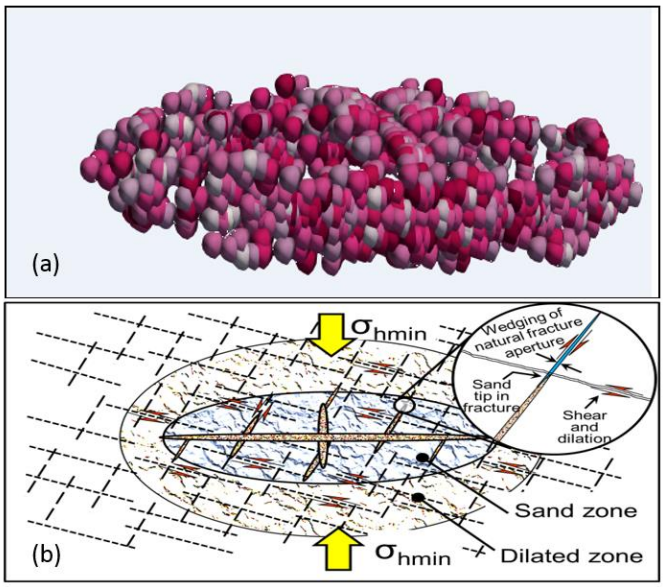

Fig. 1. (a) Example of a micorsiemic cloud distribution during the hydraulic fracturing treatment. (b) The various stimulated zones during injection into a naturally fractured system (Dusseault, 2013).

In this study, we assume that the Stimulated Volume in the jointed rock mass can be represented by an equivalent smeared poro-elastic-plastic continuum zone of enhanced permeability. Permeability is assumed to increase with increasing the effective plastic strain. A Drucker-Prager (DP) model (Drucker and Prager, 1952) is implemented within a poro-elastic-plastic Finite Element Method (FEM) framework based on Biot’s Theory (Biot, 1941). The DP failure criterion is capable to describe the Mode I and Mode II or III fracturing behavior in geomaterials.

After creation of a sufficiently large SV, the pressure fall-off analysis is carried out to quantify the various flow regimes and fracturing parameters (e.g., instantaneous shut-in pressure and fracture closure) as the natural outcome of the pressure decline analysis. For this purpose, we will use the pressure and pressure derivative diagnostic plot commonly used for draw-down and build-up well-testing interpretations. The transient analysis of the injection fall-off in a hydraulically stimulated reservoir with a sufficiently large SV has not received enough attention in the literature. This is in part due to the lack of a comprehensive geomechanical model which can describe the complex fracturing behavior of a SV and associated fluid leak-off. The large fluid leak-off volumes often create a complex fluid diffusion pattern around the leaky SV which may vary over wide range of scales from 1-D to 2-D (Sarvaramini and Garagash, 2015). Thus, the post fracturing analysis of hydraulically stimulated reservoirs using the traditional techniques, for instance, Diagnostic Fracture Injection Test (DFIT) may lead to inaccurate results. DFIT usually involves the injection of a small volume of fluid to create a small fracture followed by a period of the well-shut-in (Nolte, 1979). The small injection time scale normally minimizes the fracturing complexity and limits the fluid diffusion to the vicinity of the crack. As the result, the traditional hydraulic fracturing modeling for a single fracture with 1-D pressure dependent leak-off is sufficient to describe the fracturing behavior of a DFIT test.

One of the main objective of this study is to construct a mathematical tool for the hydraulic fracture simulation of both SV and post shut-in. The proposed methodology is expected to provide more insights on how the post-fracturing behavior of a fractured well can be related to the natural fracture distribution and micro-mechanics of damage and plasticity in the effective localized dilation zone. In this study, we will benefit from the pioneering work of Cinco-Ley (Cinco et al. 1978) to quantify the hydraulic conductivity of the SV. Cinco-Ley introduced the concept of the bi-linear flow regime for the hydraulically stimulated reservoirs with the finite fracture conductivity where the combination of linear flow in the fracture and matrix exists. It is worthwhile to mention that this flow period was initially identified for the transient pressure analysis of a single vertical fracture in the homogeneous formation and it is characterized by the quarter slope line (m=0.25) on the log-log pressure- and pressure derivative plots. As it will be shown later, the bi-linear flow period comprises a major portion of the pressure-fall-off curve for a complex SV and its characteristic can be used to find a bulk estimate of the average conductivity of the SV.

2. MATHEMATICAL FORUMATION

The poro-elasto-plastic domain is illustrated in Fig 2. The domain is bounded by its boundary $\partial\Omega$ which is composed of the sets of prescribed displacements $\partial\Omega_u$, traction $\partial\Omega_t$, flow rate $\partial\Omega_q$, pressure and plastic strain $\partial\Omega_\varrho$. The behavior of the body subjected to the given boundary conditions is described by the following equations:

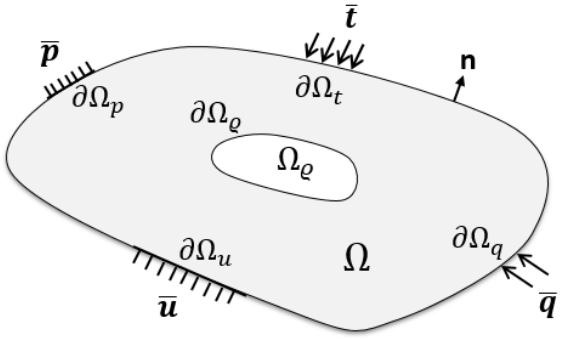

Fig. 2. Schematic of the problem domain

2.1 Equilibrium equation

The equilibrium equation and boundary conditions for the system described in Fig. 2 are

$$\nabla.(\boldsymbol{\sigma}' - \alpha \mathrm{p}\mathbf{I}) = 0 \quad (1)$$

and

$$\boldsymbol{\sigma}'.\mathbf{n}\ (\text{on}\ \partial\Omega_t) = \bar{\mathbf{t}}\ ,\mathbf{u}(\text{on}\ \partial\Omega_u) = \bar{\mathbf{u}}, \quad (2)$$

in which $\boldsymbol{\sigma}'$ is the Cauchy effective stress tensor, α is the Biot's coefficient, p is the fluid pressure, $\mathbf{I}$ is the identity tensor, and $\bar{\mathbf{t}}$ and $\bar{\mathbf{u}}$ are the prescribed traction and displacement on the boundary $\partial\Omega_t$ and $\partial\Omega_u$, respectively. Using the Hook's law, we have

$$\boldsymbol{\sigma}' = \mathbf{C}:\boldsymbol{\varepsilon}_e, \quad (3)$$

where $\boldsymbol{\varepsilon}_e$ is the elastic strain tensor and $\mathbf{C}$ is the fourth-order stiffness tensor. The elastic component in (3) can be expressed as

$$\boldsymbol{\varepsilon}_e = \boldsymbol{\varepsilon} - \boldsymbol{\varepsilon}_p \quad (4)$$

In which $\boldsymbol{\varepsilon}$ is the total strain tensor $\boldsymbol{\varepsilon}_p$ and is the plastic strain tesnor. The amount of plastic strain can be determined using an associate plastic flow rule as:

$$\boldsymbol{\Delta\varepsilon}_p = \Delta\lambda \frac{\partial f}{\partial \boldsymbol{\sigma}'} \quad (5)$$

In above, λ is the plastic multiplier and f is a yield function. In this study we use the Drucker-Prager failure criterion (Drucker and Prager, 1952) which is suitable for geomaterials, such as soil, ceramic and fractured rocks. The total strain tensor in Eq. (4) is the symmetric part of the deformation tensor given by

$$\boldsymbol{\varepsilon}(\mathbf{u}) = \frac{\mathbf{1}}{\mathbf{2}}\left(\nabla\boldsymbol{u} + \nabla\boldsymbol{u}^{\boldsymbol{T}}\right) \quad (6)$$

2.2 Continuity equation

The mass conservation of fluid within the porous medium is described by the continuity equation:

$$\frac{\partial\zeta}{\partial \mathrm{t}} + \nabla.\boldsymbol{q} = 0, \quad (7)$$

in which ζ is the fluid content and q is the fluid discharge given by the Darcy's law

$$\boldsymbol{q} = -\frac{k}{\mu}\nabla p, \quad (8)$$

where k is the permeability and μ is the injected fluid viscosity. The constitutive law relating the fluid content ζ and pressure p is expressed as

$$p = M\zeta - \alpha\ \mathrm{tr}\ (\boldsymbol{\varepsilon}). \quad (9)$$

Here, M is the Biot's modulus and tr ($\boldsymbol{\varepsilon}$) is the trace of the strain tensor. In this study k is related to plastic multiplier (λ) through an empirical correlation. The sets of initial and boundary conditions corresponding to the flow equation are:

$$\mathbf{q}.\mathbf{n}\left(\text{on}\ \partial\Omega_q\right) = \bar{\mathbf{q}},\ \mathrm{p}(\text{on}\ \partial\Omega_p) = \bar{\mathrm{p}}, \quad (10)$$

where $\mathbf{q}$ and $\bar{\mathrm{p}}$ are the prescribed flow and pressure on the boundary $\partial\Omega_q$ and $\partial\Omega_p$, respectively.

3. NUMEIRCAL SCHEME

The adopted numerical scheme to solve the system of the governing equations is based on the standard finite element Galerkin. The domain in Fig. 2 is discretized into non-structured rectangular-shaped elements. The mixed nature of the finite element problem requires the use of the 8-node quadrilateral element for displacements and 4-node quadrilateral elements for plastic strain and pressure fields to satisfy the stability condition. An implicit backward Euler scheme is used to evolve the sets of equations in time. We employ a fixed iterative solution strategy to solve Eq. (1) and Eq. (7) to compute p and u using the Newton-Raphson method. During the stress update plasticity is calculated from an appropriate plastic flow rule. The procedure is repeated until the convergence is achieved. The detail of the numerical procedure is presented in Sarvaramini et al. 2017.

4. STIMULATED VOLUME CALCULATIONS

4.1 Pre-shut-in

We consider a numerical example of water injection into a tight formation characterized by an initial porosity φ =5 %, initial virgin permeability $k_0 = 1$md, Shear modulus $G = 12$GPa, and undrained Poisson's ratio $\upsilon_u = 0.3$. The characteristic length scale which controls the natural fracture distribution and the micromechanics of fracturing is l=0.45m. The detail description of the characteristic length scale and its role on the SV evolution is given in Sarvaramini et al., 2017 and Sarvaramini et al. 2018. Water is assumed to be injected at the flow rate of $q = 10^{-4}$m^3/m.s at the center of a 200 × 200 m^2 square domain in the (x-y) plane (Fig. 3). The injection is stopped after 2000s (30 min) and the pressure is allowed to fall-off. The initial in-situ stresses are given by σ_{xx} (= σ_{min}) =-20MPa and σ_{yy} (= σ_{max}) =-40 MPa. The initial reservoir ambient pressure is $p_0 = 16$MPa. The list of the problem

parameters used in the numerical calculations is given in Table 1.

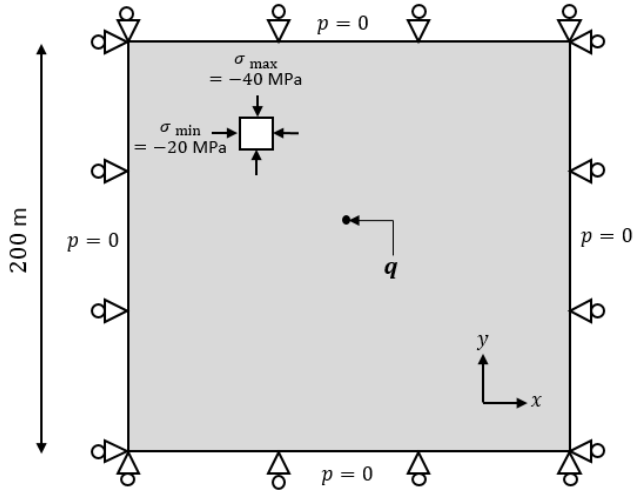

Fig. 2. Schematic of the injection problem

Table1: Material properties

Injection rate	$q = 10^{-4}$ m^3/m.s
Shear modulus	$G = 12$ MPa
Undrained Poisson's ratio	$\upsilon_u = 0.3$
Drained Poisson's ratio	$\upsilon = 0.15$
Fluid viscosity	$\mu = 1$ cp
Intermediate in-situ stress	$\sigma_V = -33.6$ MPa
Initial permeability	k_0 =1 md
Biot's coefficient	$\alpha = 0.66$
Biot's modulus	M = 29.3 GPa
Diffusivity coefficient	D = 0.2 m^2/s

Figure 3 shows the evolution of the plastic strain for the selected time steps, t=1000s and t=2000s (shut-in moment). It is evident that the injection of the fluid at the given rate has created a complex diffusive stimulated volume evolving primarily in the direction of the maximum principal stress (in this case σ_{yy} (= σ_{max}) =-40MPa), while opening against the minimum principal stress (σ_{xx} (= σ_{min}) =-20MPa). The propagation of the stimulated volume in the direction of the maximum confining stress is due to the principal of the work minimization as fracture needs less energy to propagate in the direction of the maximum principal stress. In this study, the knowledge of the initial in-situ stress field is incorporated into the model allowing one to automatically recover the fracturing path as the outcome of the numerical solution. Figure 4 shows the evolution of the net fluid pressure contours for the selected time steps. Evidently, the fluid diffusion front has extended far beyond the SV implying a two-dimensional diffusion condition. The occurrence of a two-dimensional diffusion is the result of the creation of a sufficiently large stimulated volume of enhanced permeability providing more access to the tight reservoir area (Sarvaramini and Garagash, 2016). This clearly contradicts the conventional hydraulic fracturing modeling assumption that the leak-off regime is one-dimensional, at least in the context of the complex hydraulic fracturing in the shale reservoirs. The one-dimensional leak-off assumption can be only valid in the limit of short injection time when the secondary effects from the reactivated fractures to the flow are insignificant (e.g., in the case of a mini-fracture treatment).

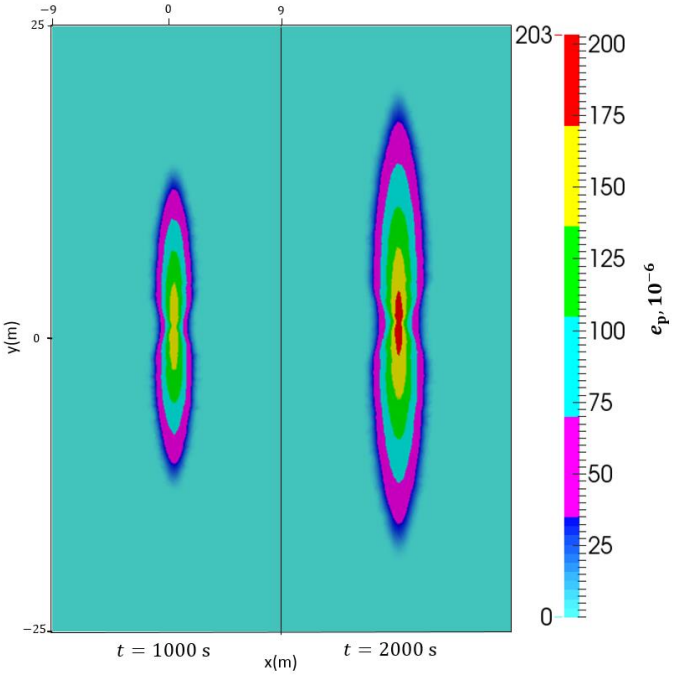

Fig. 3. Evolution of the effective plastic strain with time

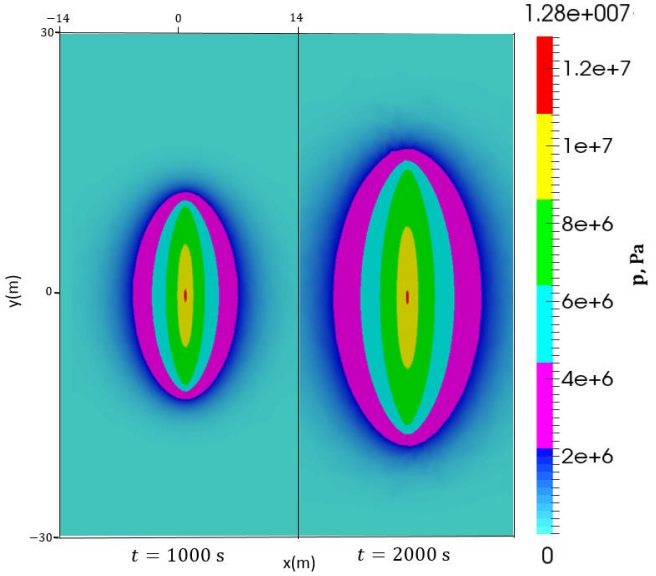

Fig. 4. Evolution of the fluid pressure with time

4.2 post-shut-in

Consider again the example of the SV evolution presented in previous section. The SV extends to about 34 meters in length in the y-direction. The injection is stopped after t_s= =2000s and the pressure is allowed to fall-off. The corresponding pressure at shut-in is p_s =12.8MPa, which in this case is equal to the stabilized fracturing propagation pressure.

Figure 5 shows the evolution of Δp (p_s-p) with Δt (t-t_s) for the pressure fall-off period. The pressure derivative type curve is also shown for comparison. Note that the pressure derivative curve in Fig. 5 is analogous to the G-function plot of a DFIT.

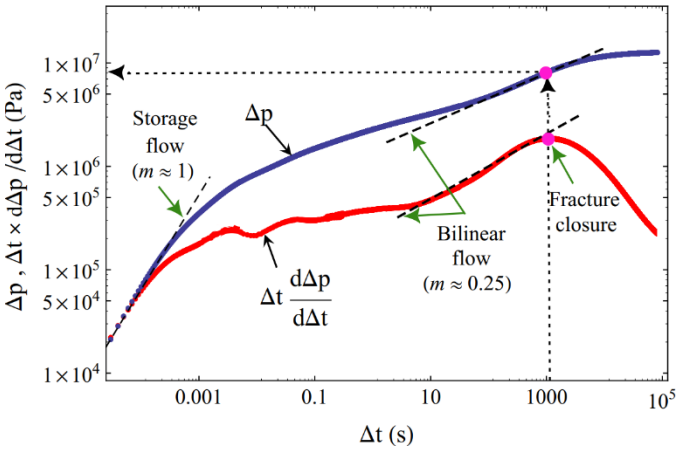

Fig. 5. pressure derivative type curves for the post injection shut-in analysis of a SV

As illustrated in Fig. 5, the pressure and derivative curves at the early period of the shut-in are characterized by a straight line of slope (m=1) suggesting that the flow regime is storage dominated. The diversion of the pressure and derivative curves from the straight line often indicates the end of wellbore and frictional effects. The pressure corresponding to the end of this flow period is commonly referred to as the instantaneous shut-in pressure (ISIP).

The most distinguished feature of the derivative curve in Fig. 5 is the characteristic 'hump' which is indicative of the fracture closure condition. The location of this maximum point can be used to identify the fracture closure pressure. Note that the fracture closure pressure and minimum in-situ stress are identical and interchangeably used. For this example, we do a crosscheck on the value of the fracture closure pressure which is expected to be at p_c= σ_{min} =20MPa. Based on the pressure derivative curve, the onset of fracture closure pressure is forecasted at Δp_c= p_s - p_c= 8.3MPa. In the view of the shut-in pressure (p_s=12.8MPa) and the initial reservoir pore pressure (p_0 =16 MPa), the corresponding final fracture closure pressure is p_c= 20.5 MPa.

Another observation of the type curves in Fig. 5 is the occurrence of the bi-linear flow regime right before the fracture closure. Bi-linear flow period was first identified in the context of fluid production from a single finite conductive fracture. The limit by which a single finite conductive fracture behaves similar to a finite conductive fracture is defined by the dimensionless flow capacity C_{fD} = $k_f w_f$ /$k_0 l_f$ <300, in which ($k_f w_f$) is the hydraulic conductivity expressed in terms of the fracture permeability k_f and fracture opening w_f, k_0 is the initial formation permeability, and l_f is the fracture half-length (Cinco et al. 1978). The bi-linear flow period is used to estimate the fracture conductivity from

$$p = \frac{q\mu\, t^{1/4}}{(k_f w_f)^{1/2} D^{1/4} k^{1/2}} \qquad (11)$$

Using Fig. 5 and the relevant parameters listed in Table 1, the estimated hydraulic conductivity is $k_f w_f$ =1.87 d.m. Assuming that the effective SV half-length is l_f =17 m, the corresponding dimensionless flow capacity is C_{fD} =110. This value implies that the hydraulic conductivity of the SV is below the threshold for which SV can be considered to be infinitely conductive.

5. CONCLUSIONS

In this article, we proposed a novel continuum mathematical approach to simulate the SV evolution and its post-fracturing behavior. We first considered an example of the SV evolution for a synthetic example of water injection into a tight formation. The evolution of the plastic strain and pressure with time were obtained. Next, we carried out the pressure decline analysis for the post-fracturing behavior of the SV. The pressure and pressure derivative curve types are used to identify the various flow regimes of the SV during the pressure fall-off period. The important fracturing parameters: fracture closure; and instantaneous shut-in pressure were also quantified as the outcome of the pressure-fall of analysis. The bi-linear flow period from the pressure type curves was used to estimate the bulk average conductivity of the SV.

REFERENCES

1. Biot M.A.: “General theory of three-dimensional consolidation”, J. Appl. Phys., pp. 155—164, 1941.

2. Boroumand N. and D.W. Eaton. Comparing energy calculations-hydraulic fracturing and microseismic monitoring. 74th EAGE Conference and Exhibition incorporating EUROPEC 2012, 2012.

3. Cinco L.H., V.F. Samaniego, and A.N. Dominguez:. Transient Pressure Behavior for a Well with a Finite-Conductivity Vertical Fracture. Society of Petroleum Engineers Journal, Trans., AIME, pp. 253-264, 1978.

4. Cipolla C.L., N.R. Warpinski, M. Mayerhofer, E.P. Lolon, and M. Vincent. The relationship between fracture complexity, reservoir properties, and fracture-treatment design. SPE production and Operations, 2010.

5. Drucker D.C. and W. Prager. Soil mechanics and plastic analysis or limit design, Quarterly of applied mathematics, pp. 157—165, 1952.

6. Dusseault M.B. J. McLennan, and J. Shu: "Massive multi-stage hydraulic fracturing for oil and gas recovery from low mobility reservoirs in China", Petroleum Drilling Techniques, pp. 6—16, 2011.

7. Dusseault M.B. Geomechanical aspects of shale gas development. Rock Mechanics for Resources, Energy and Environment, 2013.

8. Economides M.J. and K. G. Nolte. Reservoir Stimulation, 2000. John Wiley & Sons, 2000.

9. Mayerhofer M.J., E. Lolon, N.R. Warpinski, C. L. Cipolla, D. W. Walse, and C. M. Rightmire: What is stimulated reservoir volume? SPE Production and Operations, pp. 89—98, 2010.

10. Nolte K.G. Determination of fracture parameters from fracturing pressure decline. In Proceedings of the SPE Annual Technical Conference and Exhibition, Las Vegas, 1979. (SPE 8341).

11. Sarvaramini E. and D.I. Garagash. Breakdown of a pressurized fingerlike crack in a permeable solid, Journal of Applied Mechanics, pp. 061006, 2015.

12. Sarvaramini E. and D.I. Garagash. Poroelastic Effects in Reactivation of a Fingerlike Hydraulic Fracture. Journal of Applied Mechanics, pp. 061011, 2016.

13. Sarvaramini E., Maurice Dusseault, and Robert Gracie. Characterizing the stimulated reservoir volume during hydraulic fracturing-connecting the pressure fall-off phase to the geomechanics of fracturing, 2018, Journal of Applied Mechanics (Submitted).

14. Sarvaramini E., M.B. Dusseault, M. Komijani, and R. Gracie. A Non-Local Plasticity Model of Stimulated Volume Evolution during Hydraulic Fracturing, 2017, International Journal of Solids and Structures (Submitted).